Wing flexibility effects in clap-and-fling

M. Percin[1], Y. Hu[1,2], B.W.van Oudheusden[1], B. Remes[1] and F.Scarano[1]
1. Delft University of Technology, Delft, The Netherlands
2. Beihang University, Bejing, PR China

http://www.imavs.org/

ABSTRACT

The work explores the use of time-resolved tomographic PIV measurements to study a flapping-wing model, the related vortex generation mechanisms and the effect of wing flexibility on the clap-and-fling movement in particular. An experimental setup is designed and realized in a water tank by use of a single wing model and a mirror plate to simulate the wing interaction that is involved in clap-and-fling motion. The wing model used in the experiments has the same planform with the DelFly II wings and consists of a rigid leading edge and an isotropic polyester film. The thickness of the polyester film was changed in order to investigate the influence of flexibility. A similarity analysis based on the two-dimensional dynamic beam equation was performed to compare aeroelastic characteristics of flapping-wing motion in-air and in-water conditions. Based on the experimental results, the evolution of vortical structures during the clap-and-peel motion is explained. The general effects of flexibility on vortex formations and interactions are discussed. It was observed that the flexibility affects the behavior and orientation of the vortices in relation to the deformation of the wing and interaction with the mirror plate.

1 INTRODUCTION

Flapping-wing aerodynamics has been of interest to the researchers recently due to increasing design efforts in the field of Micro Aerial Vehicles (MAVs). MAVs are small unmanned air vehicles with overall dimensions not larger than 15cm [1]. Recent developments in several technological fields have enabled the possibility of using MAVs as mobile and stealth sensing platforms capable of gathering intelligence in hazardous and physically inaccessible areas. To accomplish such missions, MAVs should be capable of maneuvering with ease, staying aloft and propelling themselves efficiently. However, conventional means of thrust and lift generation become inefficient in terms of required capabilities at these scales and hence flapping-wing propulsion becomes a necessity. In contrast to the conventional mechanisms of aerodynamic force production, flapping-wing mechanisms are associated with vortices separating from the leading and trailing edge, which create low pressure region that can be used to create higher lift and thrust [1].

The phenomenon of force production as a result of flapping motion has been studied extensively in the literature originating from the pioneering studies of Knoller [2] and Betz [3], who pointed out that flapping wing motion generates an effective angle-of-attack that results in lift production with a thrust component, which is known as Knoller-Betz effect. Thenceforward, further investigations have clarified the underlying aerodynamic mechanisms, different flow topologies, and effective parameters for simplified two-dimensional flapping rigid wing motions, i.e. pitching, plunging or combined pitching-plunging. Discussion of these topics is outside the scope of the present paper and the reader is referred to [4]-[10] for more detailed information.

Natural flapping is a three-dimensional phenomenon which combines pitching, plunging, and sweeping motions [11]. Moreover, birds and insects benefit from several different unsteady aerodynamic mechanisms, among them the clap-and-fling motion, which is the particular topic of the present study.

Clap-and-fling is a lift enhancement mechanism which was first described by Weis-Fogh [12]. This relates to the wing-wing interaction phenomenon, which takes place at dorsal stroke reversal (Figure 1). During the clap phase, the leading edges of the wings come together and pronation about the leading edges occurs until the v-shaped gap between the wings disappears (see Figure 1 A-C). Subsequently, in the fling phase, the wings rotate about their trailing edges forming a gap in between. Following, the translation of the wings occurs (see Figure 1 D-F). Investigations on birds and insects showed that as well as being used continuously during the flight, some species utilize this mechanism for a limited time in order to generate extra lift, especially while carrying loads or during the take-off phase [13]. The insect experiments of Marden [14] showed that use of clap-and-fling mechanism results in generation of 25% more aerodynamic lift per unit flight muscle than conventional flapping-wing motions.

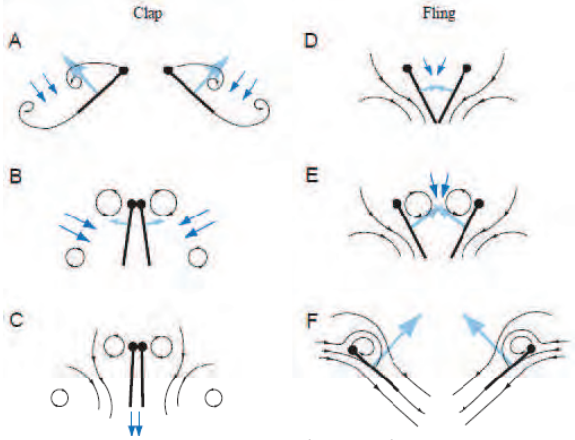

Figure 1: Schematic representation of clap-and-fling mechanism. Black lines represent flow lines, dark blue arrows show induced velocity and light blue arrows represent net force exerting on the airfoil, adapted from Sane [11].

Several studies have attempted to provide an explanation of the enhanced force generation mechanism of the clap-and-fling motion. Weis-Fogh [12] indicated that during the clap phase, as the gap between the wings vanishes progressively, the opposing circulation of both wings cancel each other out. This attenuates the starting vortex at the onset of fling and diminishes the Wagner effect. By doing so, circulation will build up more rapidly and the benefit of lift over time will be extended in the fling phase [11]. Moreover, a

http://www.imavs.org/

downward momentum jet formed at the end of clapping motion can work in favor of lift generation [15]. On the other hand, during the fling phase, as the leading edges move apart, the fluid rushes into the low pressure region between two wings, which results in generation of massive leading edge vortices. This mechanism enhances circulation at the onset of fling phase and hence increases lift. This phenomenon was experimentally verified by Lehmann et al. [16]. They performed instantaneous PIV and force measurements on dynamically scaled rigid fruit fly wings in order to investigate the effects of the clap-and-fling motion on the force production. They pointed out that clap-and-fling motion, depending on the stroke kinematics, may enhance the force production up to 17%. Detailed PIV analysis revealed that the existence of a bilateral image wing increases the circulation induced by the leading edge vortex during the early fling phase, obviously correlated with a prominent peak in both lift and drag. Furthermore, it was shown that trailing edge vorticity shed during the clap phase of the motion is considerably reduced with respect to the single flapping wing case.

It is obvious that the majority of these studies focus on the flapping motion of rigid wings and the effect of flexibility has received relatively little attention. However, studies on the mechanical properties of insect wings report complicated variations in their stiffness and identify them absolutely flexible [17], [18]. Although aerodynamic benefits of flexibility for the insect are not completely clear [19], there is a growing evidence that wing deformation during the flapping motion boosts thrust and lift production considerably [20]. Vanella et al. [21] carried out a computational study on a hovering two-dimensional flexible wing model for Reynolds number (Re) ranging from 75 to 1000. They concluded that flexibility can enhance the aerodynamic performance and the best performance was achieved when the wing was flapped at 1/3 of the natural frequency. Heathcote and Gursul [19] performed water tunnel experiments to investigate the effect of chord-wise flexibility on the propulsive efficiency of a heaving airfoil for Re of 9000 to 27000. They concluded that a certain degree of flexibility enhances the thrust coefficient and propulsive efficiency. Heathcote et al. [22] also studied the influence of spanwise flexibility and they found out that introducing a degree of spanwise flexibility affects the vortex mechanism and increases the thrust efficiency. They added that the range of Strouhal number (Sr) in which spanwise flexibility was beneficial overlaps with the range observed in nature (0.2<Sr<0.4). Based on above discussion, it can be inferred that MAVs might benefit from aerodynamic contributions of flexibility, in addition to the intrinsic low weight of flexible structures.

Regarding the clap-and-fling motion, it was shown that with the effect of flexibility the fling phase occurs more like a peel, while the clap phase can be considered as reverse-peel [23]. That is the reason why clap-and-fling motion is called clap-and-peel motion for flexible wing case. It has been speculated that flexible wings increase lift by enhancing the circulation in the fling phase and boosting the strength of downward momentum jet in the clap phase [15]. Moreover, it was indicated that flexibility reduces drag by allowing the wing to bend or reconfigure under the aerodynamic loading [24]. Miller and Peskin [24] investigated this phenomenon computationally by use of an immersed boundary method for Re of 10. They found that clap-and-fling with flexible wings produces lower drag and higher lift with respect to clap-and-fling with rigid wings.

As indicated earlier, the clap-and-fling mechanism is the particular research interest for the present paper, because of its relevance to the DelFly II, which is a bi-plane flapping-wing MAV that was designed and built at Delft University of Technology. It has four wings, of anisotropic flexible construction, undergoing clap-and-fling motion. Therefore, it is important from a design optimization point of view to obtain a better understanding of the effect of flexibility on the clap-and-fling motion.

Experimental research has been performed on the DelFly II to reveal the effect of flexibility on the aerodynamic performance. De Clercq [25] captured the instantaneous flow field in the vicinity of the flapping wings of DelFly II in hover condition via stereo-PIV and performed simultaneous thrust (viz. lift) force measurements. She showed that flexibility causes the wings to peel apart at the onset of the fling and to flex at the maximum outstroke. She also found that the peeling phase makes the major contribution to the lift thanks to the generation of massive leading edge vortices. A subsequent wing optimization study by Bruggeman [26] for the hovering condition resulted in a wing layout that provides a 10% increase in thrust-to-power ratio. Consequently, Groen [27] performed phase-locked stereo-PIV measurements to compare the deformations and flow fields for the original and the improved wing. The acquired wing shapes revealed that the improved wing in general is less flexible with respect to the original wing. This condition manifests itself also in the flow fields as shown in Figure 2. He pointed out that the LEV stays closer to the wing surface for the improved wing which was attributed to the increased suction during the peeling phase of the motion.

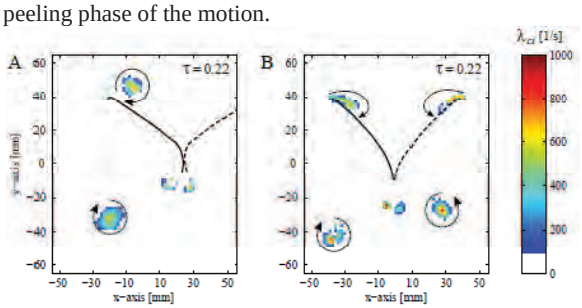

Figure 2: Comparison of swirling strengths for the original (A) and improved (B) DelFly wings flapping at 11 Hz at the spanwise position of 0.86R, adapted from Groen [27]

Notwithstanding the extensive measurements performed on the DelFly wings, it proved difficult to link the effect of flexibility to the flow field characteristics and performance improvements, due to the anisotropic characteristics of the Delfly wings and the associated complicated aeroelastic behavior. Based on these considerations, in this project it is aimed to investigate the influence of wing flexibility in a more generic configuration. The experiments were performed in a water tank to permit high-quality and time-resolved three-dimensional flow field measurements via time-resolved Tomographic Particle Image Velocimetry (TOMO-PIV) [28]. The wing model used in the experiments consists of a rigid leading edge and an isotropic flexible wing surface made from polyester film; therefore it is assumed that the wing is flexible in only the chordwise

direction. The flexibility was varied in the experiments by changing the thickness of the polyester film.

2 SIMILARITY ANALYSIS

The determination of scaling laws is an important step in order to identify characteristic properties of the system under consideration and to establish which combination of parameters is of importance for the given conditions. In the current study, analysis of structural dynamics as well as fluid dynamics becomes necessary, because of the different deformation characteristics of a flapping flexible wing for in-air and in-water conditions. The Euler-Bernoulli dynamic beam equation was utilized for the analysis of similarity parameters. The general form of the equation after neglecting the rotary inertia and deformations due to shear is shown below.

$$m\frac{\partial^2 w}{\partial t^2} + EI\frac{\partial^4 w}{\partial x^4} = f(x,t) \quad (1)$$

It should be noted that deformation only in the chordwise direction *x* is considered, in accordance with the model wing used in the experiments. In Equation-1, m is the mass per unit chord length, E is the Young's modulus, and I is the moment of inertia. The term *f(x,t)* on the right hand side is the forcing function term, consisting of aerodynamic and inertial contributions, as given in Equation-2, for a sinusoidally heaving leading edge.

$$f(x,t) = -C_{aero}\left|-\omega\bar{h}\sin(\omega t)\right|\left(-\omega\bar{h}\sin(\omega t)\right) - m\left(-\omega^2\bar{h}\cos(\omega t)\right) \quad (2)$$

Here, C_{aero} is the aerodynamic multiplication factor ($C_{aero} = 0.5\rho_f \bar{c}$, where $\bar{c}$ is the mean chord length, and ρ_f the fluid density), ω is the circular frequency ($\omega = 2\pi f$, with f the flapping frequency), and $\bar{h}$ is the amplitude of the heaving motion. Dimensional analysis of Equations-1 and 2 yields two similarity parameters, which are the ratio of elastic to aerodynamic forces (bending stiffness parameter, Equation-3), and the ratio of inertial to aerodynamic forces (Equation-4).

$$\lambda = \frac{EI}{\rho_f f^2 \phi^2 b^3 c^3} \quad (3)$$

$$\tau = \frac{\rho_w t}{\rho_f b\phi} \quad (4)$$

In this, ϕ is the angular flapping amplitude, b the span length, c the chord length (taken as the mean chord in the present calculations), ρ_w the density of the wing material, and *t* the thickness of the wing.

In addition to the derivation of similarity parameters, analytical solutions of the dynamic beam equation were used for comparison of the deformation characteristics for in-air and in-water conditions. The solution was performed for a sinusoidally plunging airfoil which is assumed to represent the cross-section of the flapping wing. Firstly, a wing of isotropic flexibility was defined as an equivalent-DelFly-wing. Secondly, a model wing for in-water conditions was defined, operating at the same Reynolds number and with similar flexibility as the (equivalent) DelFly wing.

Assumptions involved in the definition of the equivalent DelFly wing are: (1) it has the same geometry ($b = 0.14$ m, $\bar{c} = 0.08$ m, and $AR = 1.75$) and mass (88 mg for a single wing excluding the rigid leading edge) as the DelFly wing; (2) it has isotropic structural characteristics; (3) it flaps in-air at 13 Hz and (4) the maximum deformation (trailing edge displacement with respect to leading edge) it experiences is equal to that of the DelFly wing. The maximum deformation for the reference case was observed to be approximately 60% of the chord length at 71% of the span length, based on the wing shape visualization performed by Groen [27].

The analytical solution was then used to determine the required flexural stiffness of the equivalent-DelFly-wing. The maximum deformation of 60% of chord length is achieved at a flexural stiffness value of 1.06×10^{-4} Nm^2. The order of flexural stiffness agrees with the study of Combes and Daniel [18] who measured the flexural stiffness (both in the spanwise and chordwise directions) of 16 different insect wings. Based on their correlation, the chordwise flexural stiffness for the chord-length of 8 cm is estimated as approximately 10^{-4} Nm^2.

Deformation characteristics for in-water conditions were acquired for a scaled down model-wing ($b = 0.1$ m, $\bar{c} = 0.057$ m, and $AR = 1.75$). Polyester sheet was used as a wing material and, apart from reproducing the Reynolds number, it was aimed to satisfy two constraints: first to have approximately the same amount of maximum deformation during the flapping motion for in-air and in-water conditions; second to keep the bending stiffness parameters of the equivalent-DelFly-wing and the model-wing as close as possible. These conditions were satisfied for the case of model wing with a thickness of 100 μm flapping at 0.75 Hz in water. The resultant bending stiffness parameters were calculated as 0.60 for equivalent-DelFly-wing and 0.55 for the model-wing. Deformations for a flapping period are compared in Figure 3. It should be noted that although it might be possible to satisfy the above-mentioned conditions with a different flapping frequency and wing thickness, current values were selected based on the limitations regarding to the experimental setup and material availability.

http://www.imavs.org/

http://www.imavs.org/

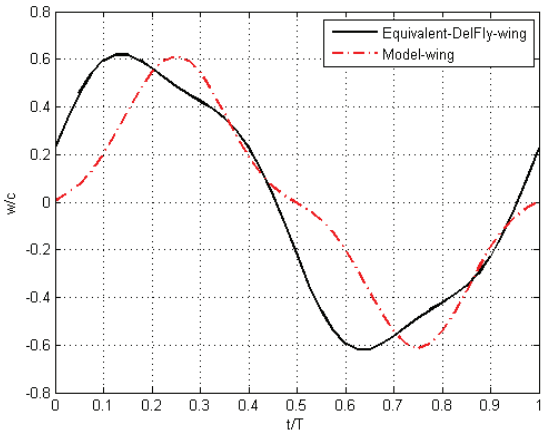

Figure 3: Comparison of total deformations (trailing edge displacement with respect to leading edge) for the equivalent-DelFly-wing flapping in air and model-wing flapping in-water

It is clear that the deformation characteristics are different from air to water, as already expected for. The major difference can be approximated by a phase shift of 10% the flapping period. In order to clarify the reason of this difference, the deformation contributions of the aerodynamic and inertial effects are shown separately in Figure 4. It is obvious that inertial forces are substantially diminished conducting experiments in water rather than air, as also evident from Equation-4. It can be concluded that the effect associated to the wing-inertia term is largely reduced when the wing flaps in water, which has similar density. As a result, it is difficult to achieve the same deformation characteristics for air and water experiments. Therefore, it is aimed to achieve order of scales of deformation and flexural bending stiffness as similar as possible to the equivalent-DelFly-wing in this study.

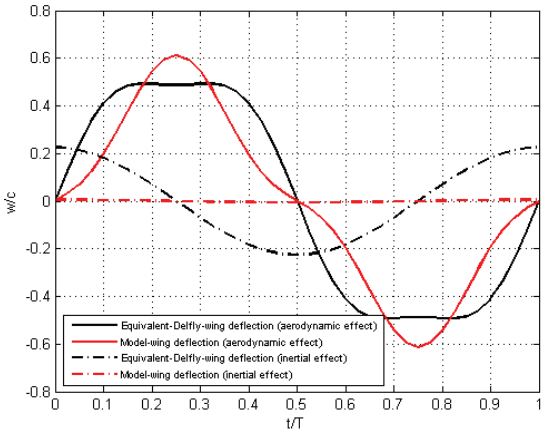

Figure 4: Comparison of deformations (trailing edge displacement with respect to leading edge) due to aerodynamic and inertial forces separately for the equivalent-DelFly-wing flapping in air and model-wing flapping in-water

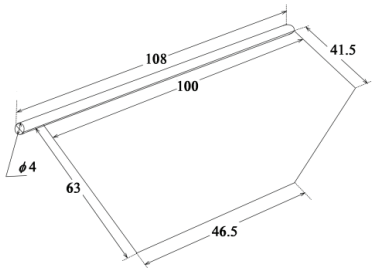

Figure 5: Dimensions of the wing model.

3 EXPERIMENTAL SETUP

Wing model and setup

The experiments were conducted in a water tank at the Aerodynamic Laboratory of Delft University of Technology (TUDelft). A single actuated wing was used in combination with a mirror plate to simulate the clap-and-fling motion of DelFly II in hovering flight. The wing model consists of a rigid leading edge and a flexible wing surface. The leading edge is made of two D-shape carbon rods of 4 mm diameter and the wing is manufactured from transparent polyester film (see Figure 5). Four different polyester wings with thickness of 50, 100, 175 and 250 μm were used to investigate the effect of flexibility.

As shown in Figure 6, a stainless steel rod with a diameter of 15 mm, connecting with the wing model, stands vertically in the octagonal water tank (600 mm of diameter and 600 mm of height). The existing water tank is made of Plexiglass allowing full optical access for illumination and tomographic imaging to study turbulent jets [29]. The distance between the rod axis and the surface of the mirror plate is 10 mm. When the motor actuates the crank-arm mechanism, the wing will flap with an amplitude of 50^o and a frequency of 0.5-1.0 Hz. Based on the mean wing tip velocity and the mean chord length, the Reynolds number for hovering flight [30] is 6700.

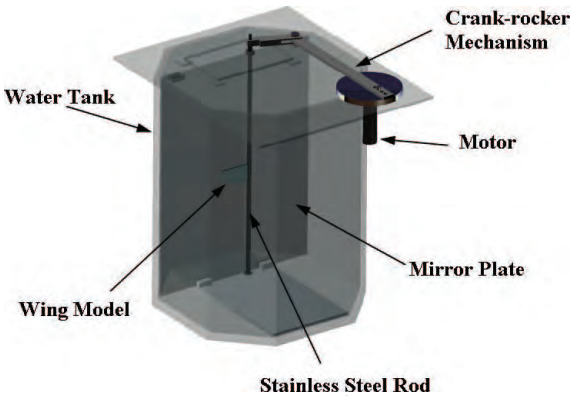

Figure 6: schematic representation of experimental set-up.

Time-resolved tomographic PIV

High-speed tomographic-PIV measurements were carried out to acquire time-resolved three-dimensional quantitative information of the flow around the wing model. Polyamide spherical particles of 56 μm diameter were employed as tracer particles at a concentration of 0.04 particles/mm^3. An

http://www.imavs.org/

alternative method to laser was applied for volume illumination, using the light beam from a normal projector, Acer PD125D DLP, which is converged by a convex lens. Position, color and size of the beam could be modified easily by Microsoft PowerPoint software on the computer. The light with lumen of 2000 ANSI from the projector is adequate to collect sufficient light scattered by the particles. The measurement volume of 100×100×40 mm^3 in size, oriented as indicated in Figure 7(b) where the distance D = 70 mm, is captured by three high-speed cameras (1024×1024 pixels) arranged along different azimuthal directions in a horizontal plane as shown in Figure 7.

The digital resolution is 10 pixels/mm and the average particle image density is approximately 0.015 particles per pixel (ppp). The tomographic recording system is composed of three CMOS cameras with a resolution of 1024×1024 pixels at 5.4 kHz. The pixel pitch of the cameras is 20 µm. Each camera is equipped with a Nikon 60 mm focal objective with numerical aperture *f*#=11. Scheimpflug adapters are used on two cameras to align the mid-plane of the measurement volume with the focal plane. Image sequences of tracer particles are recorded with recording frequency of 250 Hz (exposures time is 1/300 s).

Tomographic reconstruction

Besides synchronization of the cameras and image acquisition, DaVis 7.4 (LaVision) was also used in the image pre-processing, volume calibration, self-calibration [31], reconstruction, and three-dimensional cross-correlation based interrogation that yields the velocity vector fields.

In this experiment, the measurement volume is calibrated by scanning a plate with 9×10 dots through the volume in depth of 20 mm with steps of 5 mm. In each of the calibration planes, the relation between the physical coordinates (*X, Y, Z*) and image coordinates is described by a 3rd order polynomial fit. Linear interpolation is used to find the corresponding image coordinates at intermediate *z*-locations.

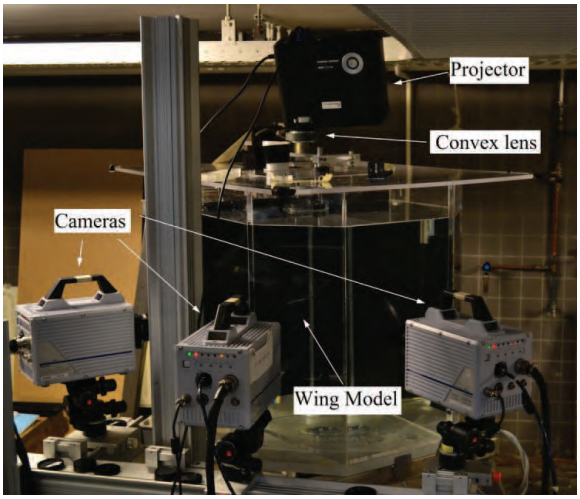

(a) Experimental arrangement in the water tank.

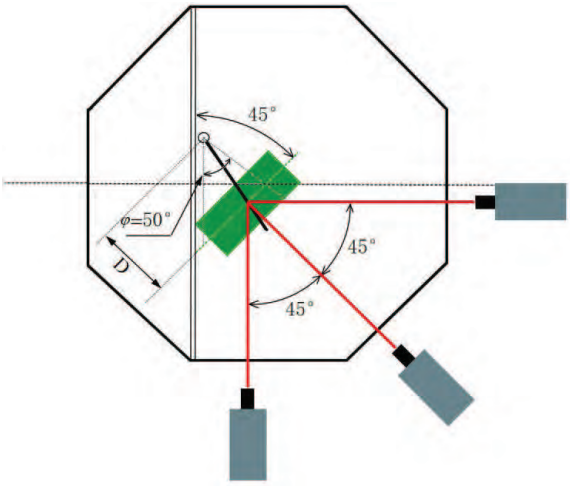

(b) Schematic representation of top view.

Figure 7: Optical arrangement for the TR-PIV experiments.

The reconstruction process is improved by means of image pre-processing with background intensity removal, particle intensity equalization and a Gaussian smooth (3×3 kernel size). Reconstructed volumes are discretized at 10^3 voxels per mm^3. The particle images are interrogated using windows of final size 64×64×64 voxels with an overlap factor of 75 %, resulting in a vector spacing of about 1.6 mm in each direction. A dataset of order 62×62×25 velocity vector volumes is acquired in each region.

4 RESULTS

Four polyester wings with different thickness (ranging from 50 to 250 µm) were used to investigate the effect of flexibility. In this section, the evolution of vortical structures at the clap-and-peel phase of the flapping motion is discussed. For brevity, only the cases of 100 and 250 µm wings flapping at 0.75 Hz are represented here.

In Figure-8, iso-surfaces of vorticity magnitude during the clap-and-peel phase are shown for the wing with a thickness of 100 µm. The end of clap is labeled as t=0 and the rear surface of the illumination volume is represented with a green slice. The wing position with respect to symmetry plane is schematized on the left corner of each phase. The vortex formation mechanism can be explained as follows: After the onset of instroke, the wing starts to move towards the wall with the formation of leading end trailing edge vortices (t=-0.12T). The separating shear layer from the trailing edge forms into a discrete trailing edge vortex. Trailing and leading edge vortices grow in size as the rotation goes on (t=-0.06T). At the end of in-stroke, the trailing edge vortex sheds into the wake of the wing, whereas the leading edge vortex stretches downward behind the wing (t=0). During the supination (t=0.06T), the stretched leading edge vortex moves towards the tapered part of the wing and interacts with the newly formed trailing edge vortex (t=0.12T). The outstroke continues with the formation of a massive leading edge vortex (t=0.16T) thanks to the inrush of fluid into the gap between the wing and the wall during the peeling phase.

http://www.imavs.org/

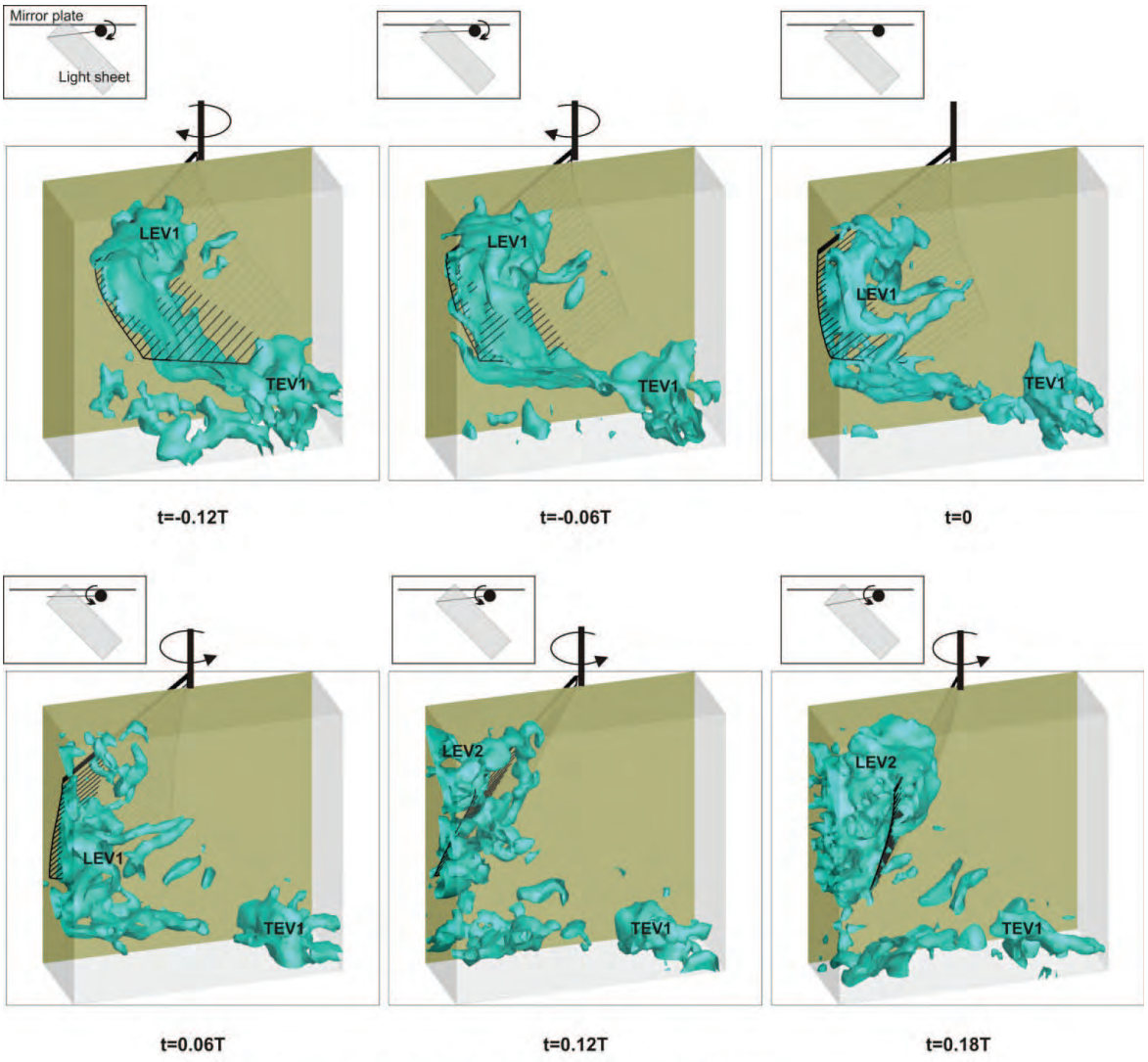

Figure 8: Isosurfaces of vorticity magnitude during the clap-and-peel phase (t=100 μm, f=0.75 Hz)

The wing flexibility manifests its effects in general vortex formation-interaction mechanisms as well as in the deformation of the wing during the flapping motion. In Figure-9, contours of z-vorticity are plotted in the cross section plane at 70% of the span at the early clap phase (t=-0.12T), for the wings with thickness of 100 and 250 μm.

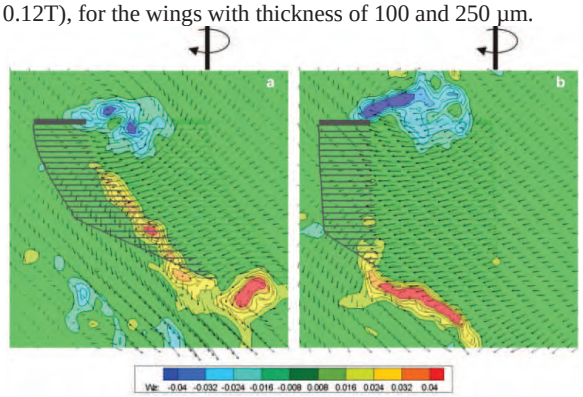

Figure 9: Contours of z vorticity for the wings at 70% of the span lengths of the wings with thicknesses of (a) 100 μm and (b) 250 μm at t=-0.12T

It is clear that the flexible wing curves towards its own wake whereas the other wing is almost rigid. In the case of the rigid wing, a stronger leading edge vortex is present but rather detached from the wing surface. It is possible to indicate that this condition will result in lower lift generation than the flexible wing case where the leading edge vortex stays near the curved surface of the wing and creates suction that works in favour of lift generation. On the other hand, the separating shear layer of the rigid wing trailing edge is curved downwards most probably due to increased downwash generated. In contrast, for the flexible wing, the trailing edge vortex stays inside the wake.

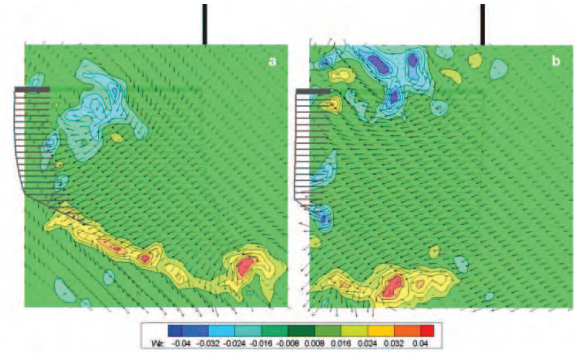

Figure 10: Contours of z vorticity for the wings at 70% of the span lengths of the wings with thicknesses of (a) 100 µm and (b) 250 µm at t=0

The vortical formations for the rigid and flexible wings are compared at the end of the clap (t=0) in Figure-10.

It is evident that due to the rigidity of the wing, the interaction with the wall results in stronger downwash and upwash (due to finite distance between the rigid leading edge and the wall) which in turn cause the vortices formed during the previous instroke to convect downward and upward, respectively. As noted earlier, contrary to the rigid wing case, the leading edge vortex in the case of flexible wing stays in the wake.

The comparison of z-vorticity contours at the late peel phase (Figure-11) reveals the fact that the rigid wing supinates into relatively stationary fluid region with respect to flexible wing case. It can be speculated that this condition will result in increase of the power requirement to fling the wing apart.

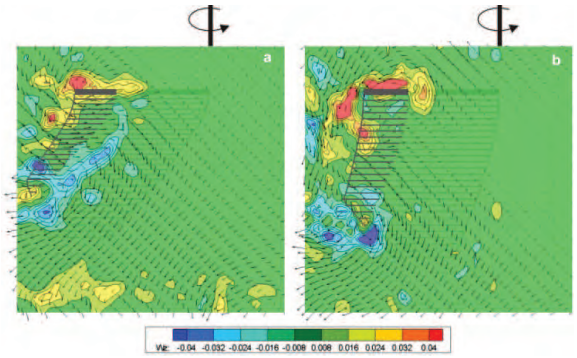

Figure 11: Contours of z vorticity for the wings at 70% of the span lengths of the wings with thicknesses of (a) 100 µm and (b) 250 µm at t=0.18T

5 CONCLUSION

The applicability of time-resolved tomographic PIV for the experimental investigation of vortical structures and effects of flexibility for the clap-and-fling type flapping motion was studied in this investigation. Experiments were performed in a water tank with a model wing that consists of a rigid leading edge and an isotropic flexible polyester film. The thickness of the polyester film was changed to investigate the influence of flexibility. A similarity analysis was performed by use of the two-dimensional dynamic beam equation. This revealed the different deformation characteristics for in-air and in-water conditions. Experimental results obtained with the tomo-PIV technique allow to characterize the three-dimensional structure of the flow field around the flapping wing model. The general vortex formation and interaction mechanisms are explained during the clap-and-peel phase of the flapping motion. It was shown that in the case of more rigid wing case, leading and trailing edge vortices stay detached from the surface of the wing and they convect upwards and downwards due to relatively strong up-downwash generated as a result of interaction with the wall. Therefore, at the stroke reversal, the more rigid wing cannot benefit from the phenomenon of the wake capture. However, in the more flexible wing case, vortices from the previous stroke interact with the wing and newly generated vortices.

REFERENCES

[1] J. Young. Numerical simulation of the unsteady aerodynamics of flapping airfoils. *The University of New South Wales Ph.D. thesis*, Sydney, 2005.

[2] R. Knoller. Die gesetze des luftwiderstandes. *Flug- und Motortechnik (Wien)*, 3(21): 1–7, 1909.

[3] A. Betz. Ein beitrag zur erklaerung des segelfluges. *Zeitschrift fur Flugtechnik und Motorluftschiffahrt*, 3: 269–272, 1912.

[4] J.M. Anderson, K. Streitlien, D.S. Barrett, and M.S. Triantafyllou. Oscillating foils of high propulsive efficiency. *Journal of Fluid Mechanics*, 360: 41-72, 1998.

[5] J.C.S. Lai, and M.F. Platzer. Jet characteristics of a plunging airfoil. *AIAA Journal*, 37(12): 1999.

[6] J. Young, and J.C.S. Lai. Oscillation frequency and amplitude effects on the wake of a plunging airfoil. *AIAA Journal*, 42(10): 2042–2052, 2004.

[7] I.H. Tuncer, and M. Kaya. Optimization of flapping airfoils for maximum thrust and propulsive efficiency. *AIAA Journal*, 43(11): 2005.

[8] J. Young, and J.C.S. Lai. Vortex lock-in phenomenon in the wake of a plunging airfoil. *AIAA Journal*, 45(2): 2007.

[9] J. Young, and J.C.S. Lai. Mechanisms influencing the efficiency of oscillating airfoil propulsion. *AIAA Journal*, 45(7): 2007.

[10] M.F. Platzer, K.D. Jones, J. Young, and J.C.S Lai. Flapping-wing aerodynamics: progress and challenges. *AIAA Journal*, 46(9): 2008.

[11] S.P. Sane. The aerodynamics of insect flight. *The Journal of Experimental Biology*, 206: 4191-4208, 2003.

[12] T. Weis-Fogh. Quick estimates of flight fitness in hovering animals, including novel mechanisms for lift production. *The Journal Experimental Biology*, 59: 169-230, 1973.

[13] F.O. Lehmann. The mechanisms of lift enhancement in insect flight. *Naturwissenschaften*, 91(3): 101 – 122, 2004.

[14] J. Marden. Maximum lift production during take-off in flying animals. *The Journal of Experimental Biology*, 130:235–258, 1987.

[15] C.P. Ellington. The aerodynamics of insect flight. IV. Aerodynamic mechanisms. *Philosophical Transactions of the Royal Society B*, 305:79–113, 1984.

[16] F.O. Lehmann, S.P. Sane, M. Dickinson. The aerodynamic effect of wing-wing interaction in flapping insect wings. The *Journal of Experimental Biology*, 208: 3075-3092, 2005.

[17] R.J. Wootton. Support and deformability in insect wings. *Journal of Zoology: Proceedings of the Zoological Society of London*, 193: 447-468, 1981.

[18] S.A. Combes, and T.L. Daniel. Flexural stiffness in insect wings I. Scaling and influence of wing venation. *The Journal of Experimental Biology*, 206: 2979-2987, 2003.

[19] S. Heathcote, and I. Gursul. Flexible flapping airfoil propulsion at low Reynolds numbers. *AIAA Journal*, 45(5): 1066-1079, 2007.

[20] P. Gopalakrishnan, and D.K. Tafti. Effect of wing flexibility on lift and thrust production in flapping flight. *AIAA Journal*, 48(5): 865-877, 2010.

[21] M. Vanella, T. Fitzgerald, S. Preidikman, E. Balaras, and B. Balachandran. Influence of flexibility on the aerodynamic performance of a hovering wing. *The Journal of Experimental Biology*, 212: 95-105, 2009.

[22] S. Heathcote, Z. Wang, and I. Gursul. Effect of spanwise flexibility on flapping wing propulsion. *Journal of Fluids and Structure*, 24: 183-199, 2008.

[23] C.P. Ellington. The aerodynamics of insect flight. III. Kinematics. *Philosophical Transactions of the Royal Society B*, 305:41-78, 1984.

[24] L.A. Miller, and C.S. Peskin. Flexible clap and fling in tiny insect flight. *The Journal of Experimental Biology*, 212: 3076-3090, 2009.

http://www.imavs.org/

[25] K.M.E. De Clercq. Flow visualization and force measurements on a hovering flapping wing MAV DelFly II. *Delft University of Technology M.Sc. thesis*, 2009.
[26] B. Bruggeman. Improving flight performance of DelFly II in hover by improving wing design and driving mechanism. *Delft University of Technology M.Sc. thesis*, 2010.
[27] M. Groen. PIV and force measurements on the flapping-wing MAV DelFly II. *Delft University of Technology M.Sc. thesis*, 2010.
[28] G.E. Elsinga, F. Scarano, B. Wieneke, and B.W. van Oudheusden. Tomographic particle image velocimetry. *Experiments in Fluids*, 41: 933-947, 2006.
[29] D. Violato, K. Bryon, P. Moore, and F. Scarano. Application of Powell's analogy for the prediction of vortex-pairing sound in a low-Mach number jet based on time-resolved planar tomographic PIV. *16th AIAA/CEAS Aeroacoustics Conference*, 2010.
[30] C.P. Ellington. The novel aerodynamics of insect flight: applications to Micro-Air Vehicles. *The Journal of Experimental Biology*, 202: 3439–3448, 1999.
[31] B. Wieneke. Volume self-calibration for 3D particle image velocimetry. *Experiments in Fluids*, 45: 549-556, 2008.

http://www.imavs.org/